Characterising a Holographic Modal Phase Mask for the Detection of Ocular Aberrations

A.D. Corbett[2], D. Gil Leyva[2], L. Diaz-Santana[1], T.D. Wilkinson[2] and J.J. Zhong[1]

1. Department of Optometry and Visual Science, City University, Northampton Square London, EC1V 0HB, UK.
2. Department of Engineering, Cambridge University, Trumpington Street, Cambridge CB2 1PZ, UK

ABSTRACT

The accurate measurement of the double-pass ocular wave front has been shown to have a broad range of applications from LASIK surgery to adaptively corrected retinal imaging. The ocular wave front can be accurately described by a small number of Zernike circle polynomials. The modal wave front sensor was first proposed by Neil et al. and allows the coefficients of the individual Zernike modes to be measured directly. Typically the aberrations measured with the modal sensor are smaller than those seen in the ocular wave front. In this work, we investigated a technique for adapting a modal phase mask for the sensing of the ocular wave front. This involved extending the dynamic range of the sensor by increasing the pinhole size to 2.4mm and optimising the mask bias to 0.75λ. This was found to decrease the RMS error by up to a factor of three for eye-like aberrations with amplitudes up to 0.2μm. For aberrations taken from a sample of real-eye measurements a 20% decrease in the RMS error was observed.

Keywords: Modal wave front sensing, Ocular aberrations

1. INTRODUCTION

Most wave front sensing in the eye samples light exiting the eye after it has been elastically back-scattered by retinal tissue. The properties of these double-pass aberrations are far removed from those of the atmosphere; varying widely within a population, with different pupil sizes and across the exit pupil[1,2]. These dynamic, large amplitude, low order aberrations present a challenge to wave front sensing if they are to be tracked at high sensitivities and bandwidths. The most popular wave front sensing techniques are interferometric and zonal measures. Interferometric measures of the wave front provide a great deal of information about the structure of the wavefront, although even for techniques not requiring a reference beam, obtaining a sufficiently stable and coherent backscattered wave front in the eye is problematic. Shack-Hartmann wave front sensors use measures of the local tip and tilt to reconstruct the wave front. Whilst the sensor is versatile, it is not optimised for the particular aberration size and mode, having a dynamic range dictated by the focal length and density of lenslets used in the sampling array.

As shown in studies of eye aberration properties[2], a modal description of the wave front is often the most desirable as only the lower order coefficients are required to provide an accurate description. Typically the Zernike circle polynomials are chosen as the mode basis set. The modal wave front sensor proposed by Neil et al.[3] allows the sizes of individual aberration modes to be measured accurately with minimal cross-talk between modes. This modal sensor has been successfully applied to the areas of two-photon and confocal microscopy[4] and three-dimensional optical memory devices[5], but to our knowledge has yet to be applied to the field of ocular wave front sensing. Typically the sensor either sequentially or simultaneously detects the amplitude of each Zernike mode present in the input aberration by monitoring the effect of applying biasing aberrations. However, the sensor has a restricted linear dynamic range when sampling multiple aberrations, although efforts have recently been made to improve on this[6].

An advantage of sampling the wave front holographically using a modal phase mask is that the sensor is then insensitive to localized opacities in the anatomical pupil plane. As each point in the replay field is composed of a sum over the contributions from each of the pixels on the SLM, the contribution from each pixel is uniformly weighted. In traditional

5th International Workshop on Adaptive Optics for Industry and Medicine, edited by Wenhan Jiang,
Proc. of SPIE Vol. 6018, 601808, (2005) · 0277-786X/05/$15 · doi: 10.1117/12.669247

zonal wave front sensing, opacities of the cornea and the variations in the scattering and absorption properties across the retina lead to a complete loss of wave front information in the shadowed region. In holographic wave front sensing however, this merely reduces the total active area contributing to each 'pixel' in the focal plane, with the result that the loss of information is distributed across the entire focal plane, rather than being localised to one particular region. Similarly, this relationship decreases the sensitivity of the output to failures of small numbers of SLM pixels.

For this work we sought to characterise the response of the modal wave front sensor to determine its useful range of operation when sensing ocular aberrations. As well as increasing the range of ocular aberrations that can be measured statically, increasing the sensor range will also increase the stability of the sensor when implemented in an adaptive correction system. For this application, a high sensitivity together with a high closed-loop bandwidth is also desirable to enable the sensor to accurately track changes in aberration size.

2. OPERATION OF THE MODAL PHASE MASK

2.1 Outline

Conceptually, the action of a modal phase mask is to split the incident phase profile, $\psi(r,\theta)$, into two beams and add a bias phase function $\Phi(r,\theta)$ to one beam and subtract the same bias $\Phi(r,\theta)$ from other (where r and θ are the polar co-ordinates in the pupil plane). The incident and mask bias phase functions can be set to be modes of the Zernike polynomial basis set, with amplitudes of **a** and **b** respectively.

$$\psi(r,\theta) = a \cdot Z_k \qquad \Phi(r,\theta) = b \cdot Z_i \tag{1}$$

If each beam then passes through a separate lens, the size of the point spread function in the focal plane will provide an indication of how closely matched the bias and input aberrations are. For a fixed mask bias aberration, the difference in intensity between the two beams at the centre of each PSF then provides and indication of the size of the incident aberration.

One practical implementation of this method is to have the incident aberrated beam falling normally onto a distorted grating (DG) and lens pair as described by Neil et al.[7]. The DG is formed by taking the bias phase profile and adding a tilt function to it.

$$f(r,\theta) = \exp\{j[\Phi(r,\theta) + \tau(r,\theta)]\} \tag{2}$$

By taking the sign of the real part of $f(r,\theta)$ this function is binarised to phases of 0 and π which describes the phase-only DG. Light passing through the DG is diffracted into multiple orders, with the first diffraction orders carrying the phase profile of the bias $+\Phi(r,\theta)$ in one order and $-\Phi(r,\theta)$ in the conjugate order. Illuminating the DG with an aberrated wave front will then produce the phase function $[\psi(r,\theta) + \Phi(r,\theta)]$ in one order and $[\psi(r,\theta) - \Phi(r,\theta)]$ in the conjugate order, with corresponding PSFs in the replay field. If the exit pupil is uniformly illuminated, the intensities of the +1 and -1 diffraction orders are given by equation 3.

$$I_{1,2}(\nu,\xi) = \frac{1}{8\cdot\pi^3}\left|\int_0^{2\pi}\int_0^1 \exp\left[jaZ_k(r,\theta) \pm jbZ_i(r,\theta) \times \exp\left[j\nu r\cos(\theta-\xi)\right] r dr d\theta\right]\right|^2 \tag{3}$$

These intensities are then integrated over the area of a pair of pinhole detectors (radius, ν_p) set in the focal plane with the difference in intensity given by:

$$\Delta W_{ik} = \int_0^{2\pi}\int_0^{\upsilon_p} I_1(\nu,\xi)\nu d\nu d\xi - \int_0^{2\pi}\int_0^{\upsilon_p} I_2(\nu,\xi)\nu d\nu d\xi \tag{4}$$

The output signal is related to the amplitude of the incident aberration through the sensitivity matrix, **S**. A general incident beam aberration, ψ(r,θ), can be described by a sum of Zernike modes

$$\psi(r,\theta) = \sum_k a_k \cdot Z_k \tag{5}$$

By sequentially biasing the mask with each of these Zernike modes, the output signal corresponding to each input aberration mode can be determined and put into a vector of values. The estimates for the input aberration coefficients can then be calculated by inverting the sensitivity matrix.

$$a = S^{-1} \cdot \Delta W_{ik} \tag{6}$$

The sensor shows a linear response for values of **a** < **b** with the maximum signal strength given when **a** and **b** have the same magnitude. For larger values of **a** larger than **b**, the signal falls off towards zero as shown in the output curve (solid line in figure 2). To ensure linearity, the values of the bias aberration (and hence the input aberration) must be assumed to be small (with terms of $O(\mathbf{b}^3)$ negligible)[3].

2.2 Sensitivity

The sensitivity of the modal sensor is the rate of change of output signal with input amplitude evaluated at **a**=0 (equation 7), and is a measure of the accuracy with which changes in the input phase can be tracked. The sensitivity matrix describes the sensitivity of the modal sensor to a given input Zernike mode Z_k for a phase mask bias of mode Z_i (the design mode). Ideally, this matrix would appear as an identity matrix, with zero cross-talk between modes. A mathematical analysis of the sensor shows that for values of b which are sufficiently small (i.e. where terms of order $\mathbf{b}^2$ are negligible), some of the entries in the sensitivity matrix are necessarily zero whilst other off-diagonal elements are limited to being smaller than of order $\mathbf{b}^3$. By substituting equation 3 into equation 7, we have a method of being able to calculate the sensitivity for a given mask bias and pinhole size directly (equation 8).

$$S_{ik} = \left.\frac{\partial \Delta W_{ik}}{\partial a}\right|_{a=0} \tag{7}$$

$$\left.\frac{\partial I_{1,2}}{\partial a}\right|_{a=0} = \frac{1}{4 \cdot \pi^3} \mathrm{Im}\left\{ F.T.\left[\exp\left(\pm jbZ_i(r,\theta)\right)\right] \cdot F.T.\left[\tilde{Z}_k \exp\left(\mp jbZ_i(r,\theta)\right)\right]\right\} \tag{8}$$

where F.T. represents the Fourier Transform.

2.3 SLM implementation

The modal sensor can be implemented using a SLM to display the distorted grating pattern. This temporal multiplexing implementation of the sensor sequentially displays the different design modes on the SLM allowing the signal outputs for each mode to measured in turn. To investigate the effects of a limited spatial bandwidth on the dynamic range and sensitivity of the sensor the SLM was simulated using a 64x64 matrix of pixel elements. By using such a small number of pixel elements it was hoped that more could be understood about the fundamental limitations of using a diffractive approach to the wave front sensing of large aberrations. A typical mask design and its replay field are shown in figure 1.

An alternative implementation also described by Neil et al.[3] is to spatially multiplex the conjugate first orders in the replay field. The holograms used to create these diffraction orders can be calculated using optimisation routines. In the interests of speed and simplicity and in consideration of the limitations on the SLM spatial bandwidth, the modes were instead temporally multiplexed. As mentioned above, in the context of using the sensor in an adaptive corrective loop,

the closed loop bandwidth is a key design parameter. Using a ferroelectric SLM, a practical implementation of a temporally multiplexed sensor measuring seven Zernike modes and using pinhole detectors would allow an open-loop sensor bandwidth of the order of kHz.

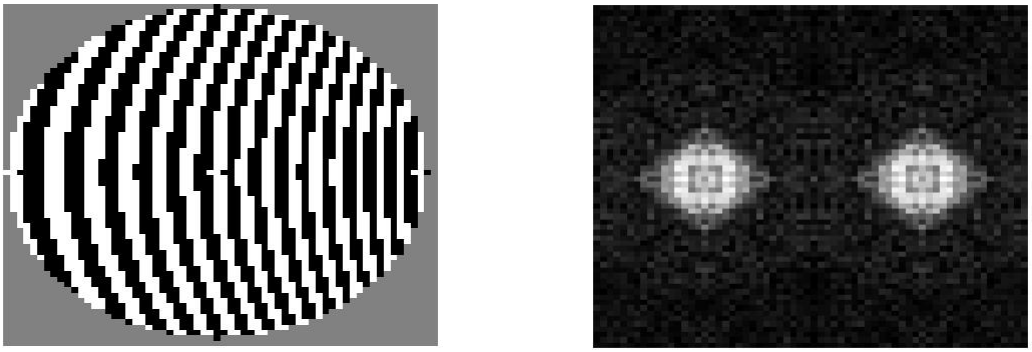

(a) (b)

Figure 1. (a) A typical mask design (black and white stripes show [0,π] phase modulation) and (b) the simulated replay field of the same mask.

3. ADAPTING THE PINHOLE SIZE TO INCREASE DYNAMIC RANGE

3.1 Effect of pinhole size on dynamic range

From the above description of the biasing method, we can see that the maximum in the intensity detected by a pinhole detector occurs when the point spread function is as localised as possible. This will also mark the point at which the maximum in the differential output signal is observed. This condition arises when the SLM is configured with a bias of exactly the size and mode required to conjugate the incident aberration. Therefore, the size of the mask bias will determine the maximum size of the incident aberration before saturation of the output signal, thereby providing an upper bound on the dynamic range of the sensor. With this in mind, the output curves for progressively larger biases and fixed pinhole size are plotted in figure 2.

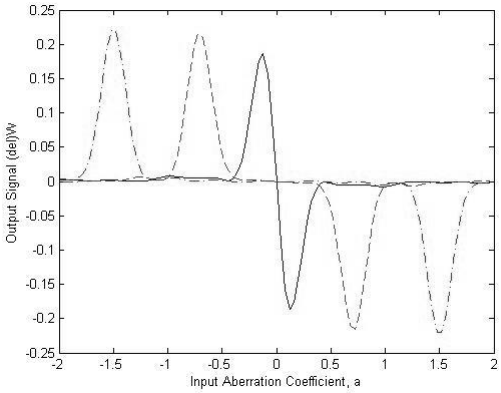

Figure 2: The sensor output signal for Zernike mode 5, with a pinhole size of 150μm and biases of 0.1λ (solid line) 0.7λ (dashed) and1.5λ (dash-dot).

As can be seen from figure 2, the effect of increasing the bias, whilst keeping the size of the pinhole detector fixed, is to completely lose the linearity of the sensor between the output signal saturation points. For most aberration sizes between the values of the bias, the sensitivity is close to zero. The reason for this effect can be understood by looking at the behaviour of the point spread function that falls over the pinhole detectors as the input aberration is increased. As the phase conjugation moves away from the ideal condition of a=b, the point spread function rapidly broadens, with the

intensity measured at the very centre of the PSF rapidly becoming flatter (figure 3). The on-axis intensity at the conjugate diffraction orders is then given by two points in figure 3, a distance of 2a apart, at (b-a) and (b+a). When |b±a| is large, the intensity is close to its asymptotic value of zero at both points, producing a negligible differential.

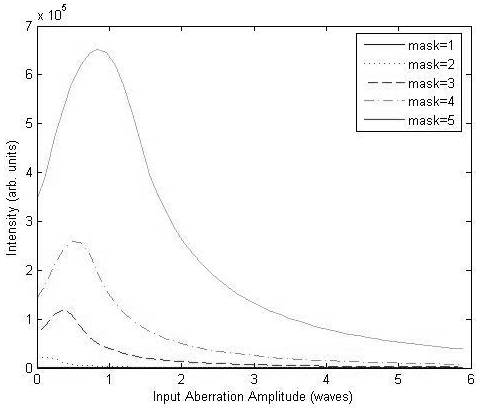

Figure 3: The change on-axis intensity measured in the replay field for pinhole sizes of 1,3,6,9,and 15*(150μm).

From figure 3 we can see that this can be overcome by increasing the size of the pinhole to increase the intensity in each detector, producing an intensity which has not decayed away to zero at large values of |(b±a)|. Taking this approach allows the differential intensity to remain non-zero as the size of the incident aberration approaches zero. This implies that in order to extend the dynamic range of the sensor, we require more information about the PSF than can be recovered from a single point measurement and that the size of the pinhole should be increased.

3.2 Choosing the bias to maximise sensitivity

Considering again the relationship between the pinhole size and the PSF, we can see that if the pinhole is much bigger than the PSF of the bias aberration there will be no change in the detector signal for small input aberrations. The sensitivity of the sensor is then practically zero for small values of a. However, if the bias aberration PSF is larger than the pinhole, the sensitivity (which is defined at a=0) will be non-zero, but as we have seen, the dynamic range will be more limited. This implies that for a given pinhole size, the bias can be optimised to maximise the sensitivity.

It was decided to select a range of pinhole sizes and then select the value of the bias which produced the greatest sensitivity (calculated using equations 7 and 8) in each case. This acted to maximise the on-diagonal elements of the sensitivity matrix, increasing the accuracy with which aberrations could be tracked. Five pinhole sizes were chosen, with values which ranged from 150μm-2.3mm (λ=632nm, pixel pitch=13μm, f=20cm). The maximum pinhole size was chosen as being that which would extend from the location of the first to the zeroth diffraction order in the replay field as pinhole sizes greater than this would be impossible to implement experimentally. For each of these pinhole sizes, the variation in sensitivity with the size of the bias aberration was calculated. The form of the curve varied according to the aberration mode (figure 4 (a)-(d)). This variation in the sensitivity curve between modes increased for larger pinhole sizes. In order to determine the optimum bias for the phase mask, a merit function was formed from the product of the sensitivity curves for each of the modes. This showed a sharp peak in the sensitivity for a particular bias value (figure 4 (e),(f)). The pinhole sizes and the optimum biases are shown in the table below. The five pinhole and bias combinations have been labelled as sensors 1-5, with output curves shown in figure 5.

Sensor Label	1	2	3	4	5
Pinhole Size (/150μm)	1	3	6	9	15
$b_{optimum}$ (λ)	0.12	0.24	0.52	0.76	1.24

Table 1: The values of the pinhole sizes and the mask bias chosen to optimise the sensitivity.

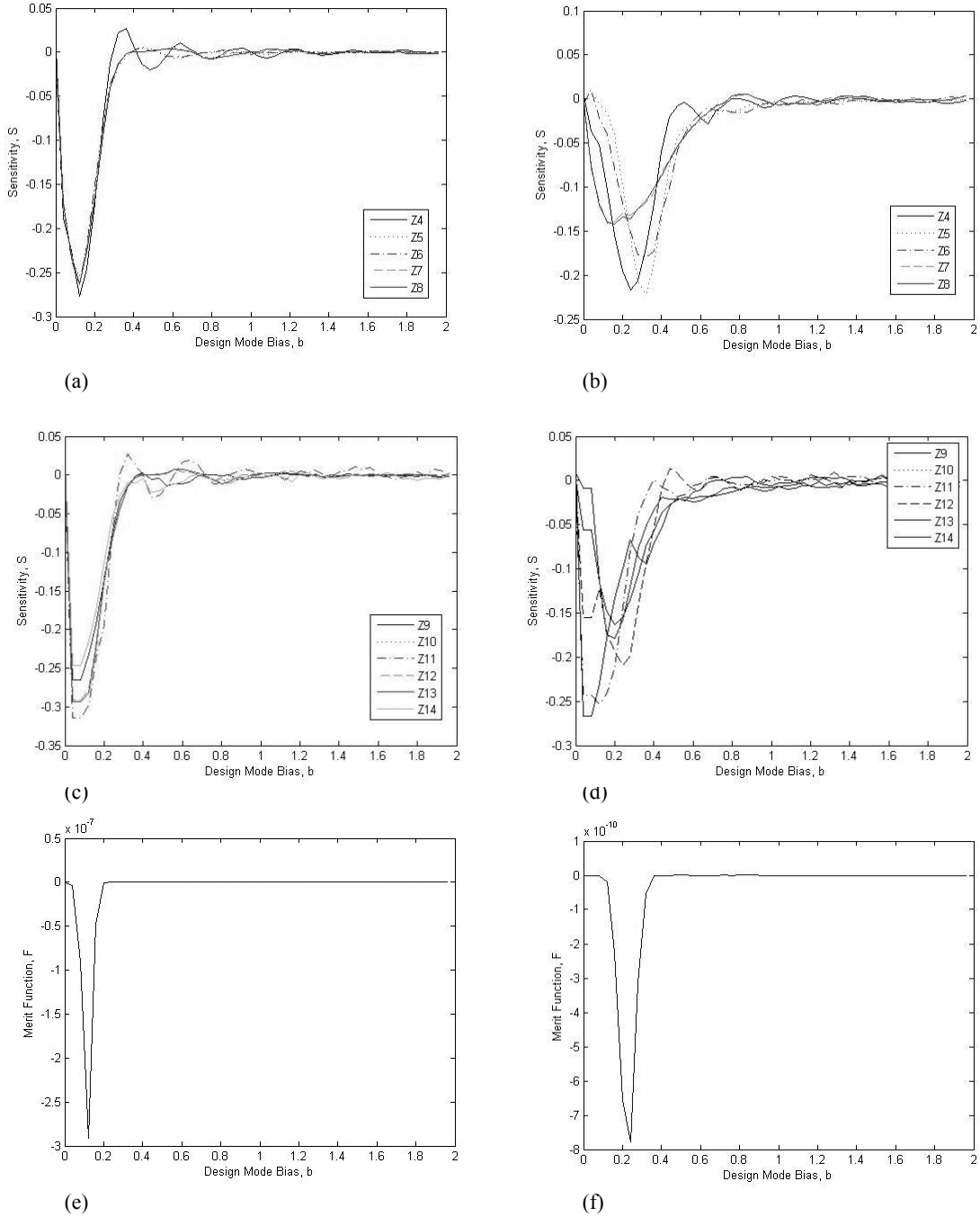

Figure 4. The variation in sensitivity with bias value for pinhole sizes 150μm and 450μm for modes 4-8 (a), and (b) modes 9-11 (c),(d). The merit functions calculated for these pinhole sizes are shown in (e) and (f).

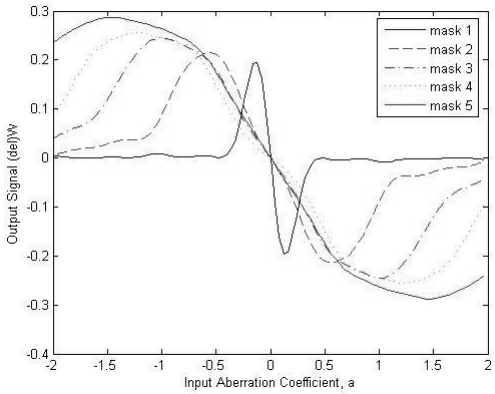

Figure 5: The output curves for each of the sensor designs.

3.3 Effect of increasing the pinhole size on the sensitivity and cross-talk.

For each of the sensor designs, the sensitivity matrix was evaluated. The sensitivity matrix for sensor 1, 3, and 5 are shown in figure 6. These matrices demonstrate the decrease in the sensitivity values along the leading diagonal of the matrix and the increase in the cross-talk as the pinhole size is increased. This can be understood by considering that the region covered by the pinholes will not only be illuminated by the first diffraction orders of the mask, but also by noise orders arising from higher diffraction orders and the pixilation of the SLM. As the pinhole increases in size, these noise orders become more prevalent and degrade the linearity of the sensor response. This leads to the decrease in the amplitude of the diagonal components in the sensitivity matrix. Similarly, as the size of the pinhole increases, more of the PSF from the conjugate first order leaks into the detector area, thereby increasing the cross-talk between the modes.

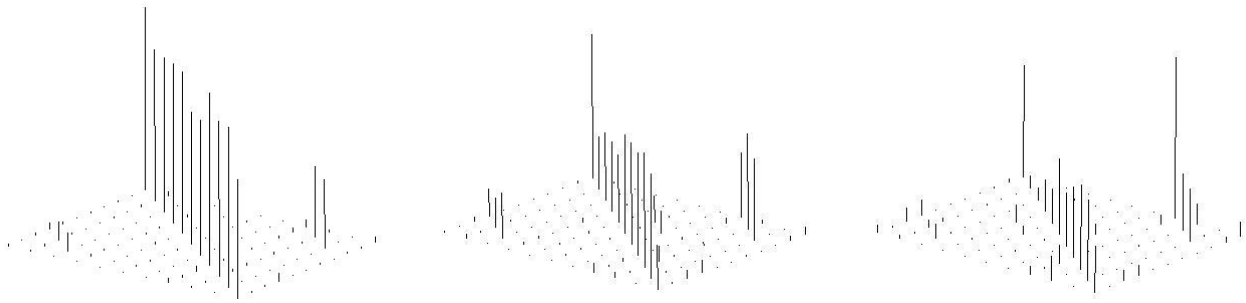

(a) (b) (c)

Figure 6. Sensitivity matrices for sensors (a) 1, (b) 3 and (c) 5. The maximum sensitivity values in each matrix are 0.31, 0.14, 0.12 respectively.

3.4 Testing the masks with real data

In order to test the ability of the modal sensors to accurately detect ocular aberrations, data was taken from a set of ocular double-pass wave fronts measured at City University. These phase fronts had been measured using the WASCA commercial optometry measurement system, based on the Shack-Hartmann wave front sensing principle. The data set was composed of three repeated measurements of each eye from a normal population of 94 subjects. The data is presented as the coefficients of the Zernike polynomials up to fourth order (Z_2-Z_{14}) of which modes 4-10 were used in the experiment. For a given subject, the average coefficient value and the standard deviation was also calculated for each mode. The distribution of mean values for each Zernike mode can be seen in figure 7 to follow a Gaussian distribution with zero mean as seen in previous studies[1]. The mean and standard deviation values for each of the Zernike polynomial coefficients across all the subjects are given below.

Zernike Mode	4	5	6	7	8	9	10
Mean Value (μm)	-0.0647	0.0946	0.0642	-0.0235	-0.0452	-0.0164	0.1445
Std. Dev. (μm)	1.2355	0.5597	0.3267	0.1301	0.2005	0.1269	0.1645

Table 2. The City data set mean values and standard deviations of the Zernike polynomial coefficients for modes 4-10.

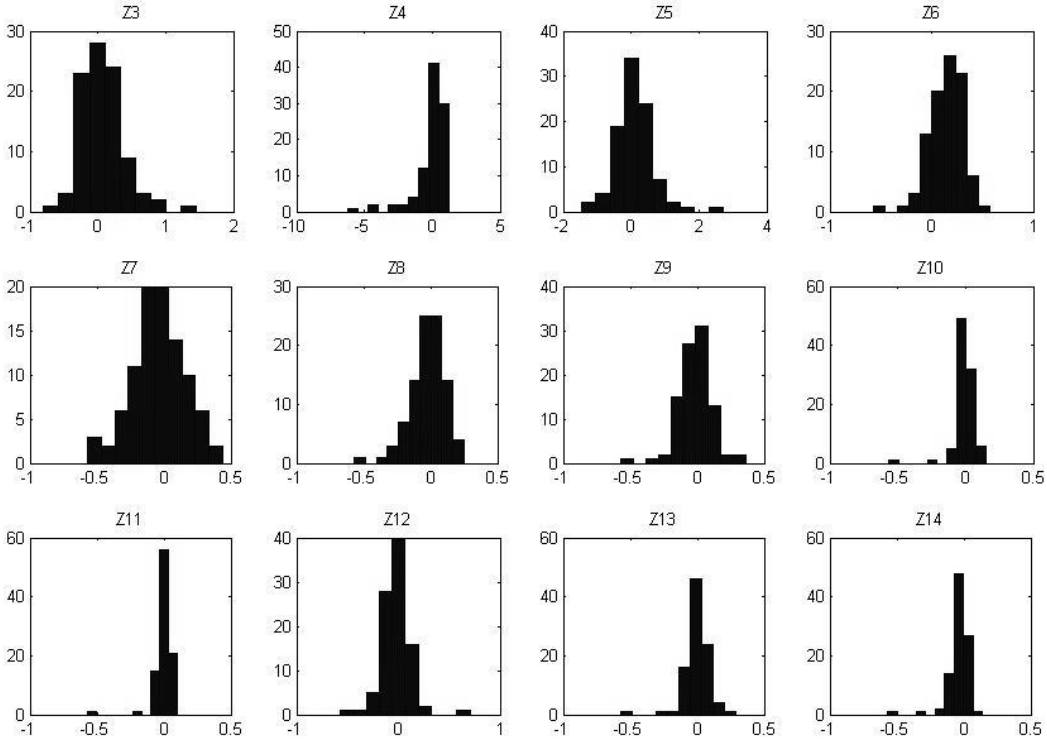

Figure 7: Histograms showing the frequency of the aberration sizes (in microns) for the City data set for Zernike modes 2-14.

The aberration for each eye was approximated by summing the Zernike polynomials (evaluated across a 64x64 grid) weighted by the mean coefficients for each subject. This phase screen was then multiplied by the phase mask of each Zernike mode of a particular sensor design and the intensities across the detector areas in the replay field evaluated. The differential intensities from each mode of given sensor design was used to form an output signal vector. Multiplying this vector by the inverse of the sensitivity matrix gave an estimate of the amplitude of the input coefficients. The RMS difference between the predicted and actual coefficients was then evaluated for each subject.

To investigate the effect of the input aberration size on the accuracy of each of the sensors, the polynomial coefficients for the City data set were scaled to values in the range [0 T] where T took the values of 0.1, 0.2, 0.4 and 0.7 microns. In addition, to determine the ability of the sensors to detect aberrations much larger than those anticipated in a typical population, coefficient values twice the size of the raw data were also used. The results for each of these data sets are shown in figure 8.

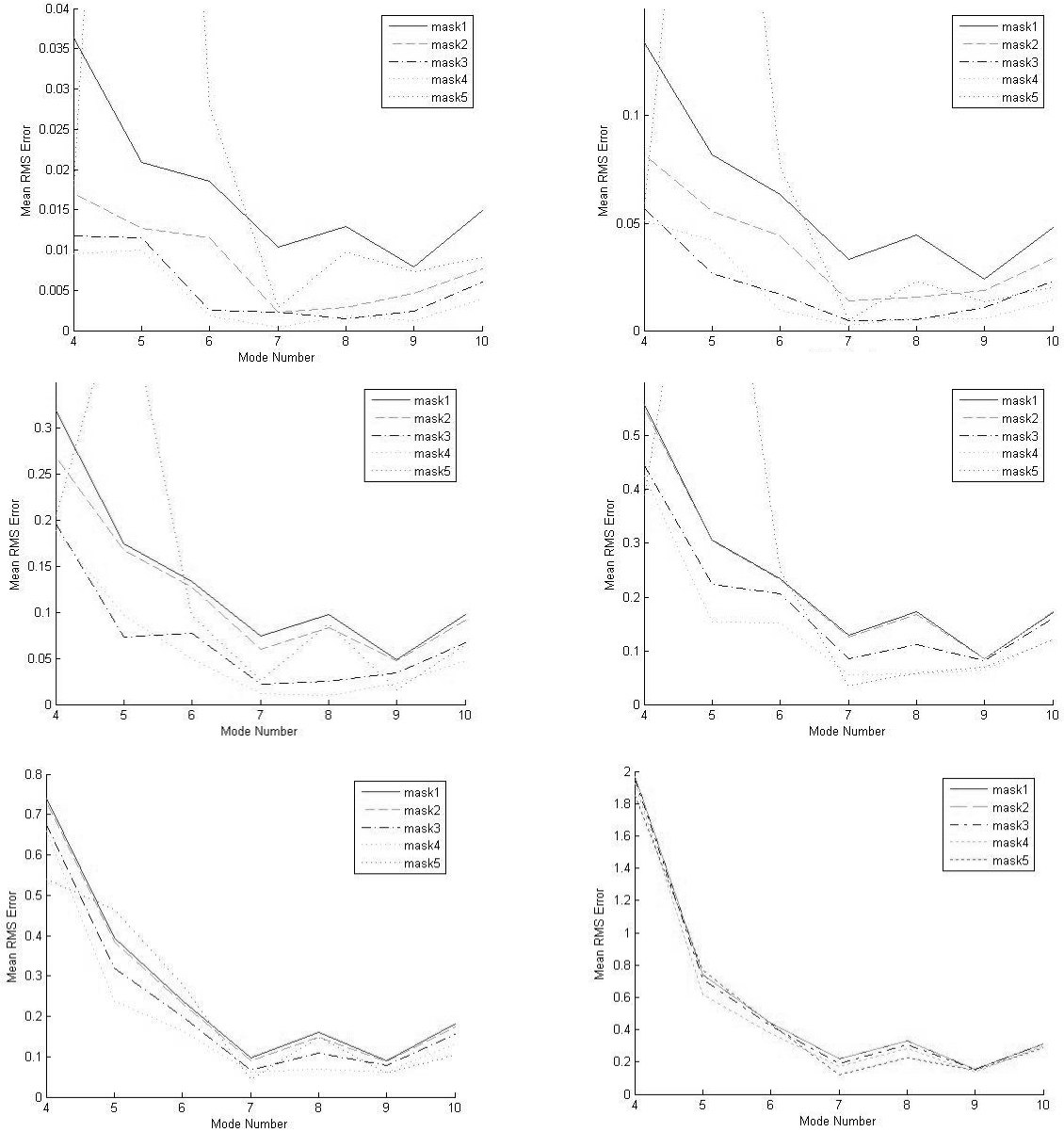

Figure 8. The RMS error values for the difference between the predicted and actual input aberration coefficients for the City data set of 94 subjects. The results shown are for the City data set with coefficient values scaled to lie within the range [0 T] with (a) T=0.1μm (b) T=0.2μm (c) T=0.4μm (d) T=0.7μm. (e) Results for the unscaled, raw coefficients and (f) scaled to twice the actual values.

4. DISCUSSION

The results demonstrated that in general the larger pinhole sizes acted to increase the dynamic range to make measurements of each mode which were accurate for a greater proportion of the subjects in the data set. This increased accuracy, expressed as a reduction in the RMS error, despite the increase in cross-talk between modes for larger pinholes, demonstrated the importance of an increased dynamic range in being able to provide a coarse estimate of the aberration size. As was expected, for the data sets scaled to sizes beyond the dynamic range of the sensors 1 and 2, the RMS errors were higher than for sensors 3, 4 and 5. The difference in the RMS errors in this case was not dramatic as

only the largest, lower order aberrations in each subject of the data set pushed the sensor beyond its range, with the majority of aberrations lying close to zero (figure 7).

Notably, the RMS error for sensor 5 was greater than for any of the other sensors for most of the aberration modes and data set scalings. This was due to the poor sensitivity to small aberrations which constitute the majority of the input aberration sizes and significant levels of cross-talk, as shown in figure 6. The RMS error results do not allow the relative size of the contribution from these two factors to be calculated exactly. However, the data does demonstrate that the broad dynamic range was shown to be more important than poor sensitivity and cross-talk for the largest aberration data sets, with sensors 4 and 5 providing the lowest RMS error. The general trend shown in figure 8 also demonstrates that as the incident aberrations grow ever larger, each of the sensors slowly saturates as their dynamic range is exceeded by a greater and greater proportion of input aberrations until each of the sensors are equally limited in their ability to detect the incoming aberrations and the plots converge in figure 8(e).

One result that was not expected was that the difference between the sensor configurations was most notable for the aberrations which were scaled to lie within the smallest range (T=0.1μm). It was anticipated that these results would have the lowest RMS error for the sensor with the smallest pinhole as the aberration sizes all fell within the dynamic range of the sensor and it had the highest sensitivity. One hint as to the possible reason for this is that the sensors with the larger pinholes had flatter RMS error curves. As the lower order mode amplitudes are generally larger than the higher order modes, this may demonstrate that sensor accuracy decreases as the aberration size approaches the limits of the sensor range and that by extending the range well beyond that of the incident aberration, accuracy may be improved.

5. CONCLUSION

We have demonstrated a method for extending the dynamic range of a modal phase mask to closer match that of a typical population of double-pass ocular wavefronts. To increase the dynamic range the bias had to be increased, but in order to maintain a non-zero differential intensity, the pinhole size also had to be increased accordingly. A range of pinhole sizes were chosen and the value of the mask bias chosen to maximise the sensitivity of the particular sensor configuration across all Zernike modes.

The results show that for a fixed number of active SLM pixels making up the modal mask, the accuracy of a sensor for detecting eye-like aberrations can be improved by increasing the pinhole size and thereby the dynamic range. However, the extent to which this is applicable is determined by the levels of cross-talk. Through increased separation of the first diffraction orders and by employing techniques from computer generated holography to suppress noise orders in the detector region, the effects of cross-talk can be minimised. These methods will in general place a greater demand on the spatial bandwidth of the SLM and require a greater number of active pixels. In the context of adaptive optics, sensors with a larger dynamic range would enable close-loop correction for a larger range of subjects. Once in stable operation, the corrective element will act to decrease the aberration size seen by the sensor. The most accurate sensor will then be one with smaller dynamic range and highest sensitivity. This implies that for adaptive optics, a sensor that can adapt with the aberration size would be most useful. Whilst the bias can be easily adjusted when using a SLM, the variation in pinhole size could be implemented by changing the region analysed in a CCD image of the mask replay field. This would then increase the accuracy, at the cost of closed-loop bandwidth and a compromise between the two must be sought.

REFERENCES

1. Thibos, L.N., et al., “Statistical variation of aberration structure and image quality in a normal population of healthy eyes.” J. Opt.Soc. Am. A, 19(12): p. 2329-2348. 2002
2. Hofer, H., et al., “Dynamics of the eyes wave aberration.” J. Opt.Soc. Am. A, 18(3): p. 497-506. 2001
3. Neil, M.A.A., M.J. Booth, and T. Wilson, “New modal wave-front sensor: a theoretical analysis.” J. Opt.Soc. Am. A, 17(6): p. 1098-1107. 2000
4. Neil, M.A.A., M.J. Booth, and T. Wilson, “New Modal Wave-Front Sensor: Application to adaptive confocal fluorescence microscopy and two-photon excitation fluorescence microscopy.” Optical Society of America, 19(10): p. 2112-2120. 2002

5. Neil, M.A.A., et al., “Active aberration correction for the writing of three-dimensional optical memory devices.” Applied Optics, 41(7): p. 1374-1379. 2002
6. Booth, M.J. “Direct Measurement of Zernike aberration modes with a modal wavefront sensor.” in SPIE Proceedings Advanced Wavefront Control: Methods, Devices, and Applications. 2003.
7. Neil, M.A.A., M.J. Booth, and T. Wilson, “Dynamic wave-front generation for the characterisation and testing of optical systems.” Optics Letters, 23(23): p. 1849. 1998